Article:
Brunet, M., Podolyák, Zs, Berry, T. A. et al. (46 more authors) (2021) Competition between allowed and first-forbidden β decays of at 208 and expansion of the Po 208 level scheme. Physical Review C - Nuclear Physics. 054327. ISSN 2469-9993

https://doi.org/10.1103/PhysRevC.103.054327

Competition between allowed and first-forbidden β decays of ^{208}At and expansion of the ^{208}Po level scheme

M. Brunet,[1,*] Zs. Podolyák,[1] T. A. Berry,[1] B. A. Brown,[2] R. J. Carroll,[1] R. Lica,[3,4] Ch. Sotty,[4,5] A. N. Andreyev,[6,7] M. J. G. Borge,[3] J. G. Cubiss,[3,8] L. M. Fraile,[8] H. O. U. Fynbo,[9] E. Gamba,[10] P. Greenlees,[11] L. J. Harkness-Brennan,[12] M. Huyse,[5] D. S. Judson,[12] J. Konki,[11] J. Kurcewicz,[3] I. Lazarus,[13] M. Madurga,[3] N. Marginean,[4] R. Marginean,[4] I. Marroquin,[14] C. Mihai,[4] E. Nácher,[15] A. Negret,[4] S. Pascu,[4] R. D. Page,[12] A. Perea,[14] J. Phrompao,[16] M. Piersa,[17] V. Pucknell,[13] P. Rahkila,[11] E. Rapisarda,[3] P. H. Regan,[1,18] F. Rotaru,[4] M. Rudigier,[1] C. M. Shand,[1] R. Shearman,[1,18] E. C. Simpson,[19] T. Stora,[3] O. Tengblad,[14] P. Van Duppen,[5] V. Vedia,[8] S. Vinals,[14] R. Wadsworth,[6] N. Warr,[19] and H. De Witte[5]

[1]*Department of Physics, University of Surrey, Guildford GU2 7XH, United Kingdom*
[2]*Department of Physics and Astronomy and National Superconducting Cyclotron Laboratory, Michigan State University, East Lansing, Michigan 48824-1321, USA*
[3]*Physics Department, CERN, 1211 Geneva 23, Switzerland*
[4]*H. Hulubei National Institute for Physics and Nuclear Engineering, Strada Reactorului 30, Măgurele, Romania*
[5]*KU Leuven, Institut voor Kern- en Stralingsfysica, Celestijnenlaan 200D, 3001 Leuven, Belgium*
[6]*Department of Physics, University of York, North Yorkshire YO10 5DD, United Kingdom*
[7]*Advanced Science Research Center (ASRC), Japan Atomic Energy Agency (JAEA), Tokai-mura, Naka-gun, Ibaraki 319-1195, Japan*
[8]*Grupo de Física Nuclear & IPARCOS, Universidad Complutense de Madrid, CEI Moncloa, 28040 Madrid, Spain*
[9]*Department of Physics and Astronomy, Aarhus University, DK-8000 Aarhus, Denmark*
[10]*School of Computing, Engineering, and Mathematics, University of Brighton, Brighton BN2 4GJ, United Kingdom*
[11]*Department of Physics, P.O. Box 35 (YFL), University of Jyväskylä, FI-40014 Jyväskylä, Finland*
[12]*Department of Physics Oliver Lodge Laboratory, University of Liverpool, Liverpool L7 7BD, United Kingdom*
[13]*STFC, Daresbury Laboratory, Warrington WA4 4AD, United Kingdom*
[14]*Instituto de Estructura de la Materia, CSIC, Serrano 113 bis, E-28006 Madrid, Spain*
[15]*Instituto de Física Corpuscular, CSIC–Universidad de Valencia, E-46980 Valencia, Spain*
[16]*Max-Planck-Institut für Quantenoptik, Hans-Kopfermann-Straße 1, D-85748 Garching, Germany*
[17]*Faculty of Physics, University of Warsaw, PL 02-093 Warsaw, Poland*
[18]*National Physical Laboratory, Teddington, Middlesex TW11 OLW, United Kingdom*
[19]*Department of Nuclear Physics, Research School of Physics, Australian National University, Canberra, ACT 2601, Australia*

(Received 22 October 2020; revised 23 March 2021; accepted 29 April 2021; published 28 May 2021)

The structure of ^{208}Po populated through the EC/β^+ decay of ^{208}At is investigated using γ-ray spectroscopy at the ISOLDE Decay Station. The presented level scheme contains 27 new excited states and 43 new transitions, as well as a further 50 previously observed γ rays which have been (re)assigned a position. The level scheme is compared to shell model calculations. Through this analysis approximately half of the β-decay strength of ^{208}At is found to proceed via allowed decay and half via first-forbidden decay. The first-forbidden transitions predominantly populate core excited states at high excitation energies, which is qualitatively understood using shell model considerations. This mass region provides an excellent testing ground for the competition between allowed and first-forbidden β-decay calculations, important for the detailed understanding of the nucleosynthesis of heavy elements.

DOI: 10.1103/PhysRevC.103.054327

I. INTRODUCTION

The proximity of ^{208}Po to the doubly magic ^{208}Pb nucleus makes it an excellent tool to test the shell model. With two-proton particles and two-neutron holes, its low-energy level scheme is characterized by excited states of predominantly neutron and proton character. At higher energies additional unpaired protons and neutrons contribute and the wave functions become more fragmented.

By populating ^{208}Po via the EC/β^+ decay of its parent nucleus ^{208}At ($J^\pi = 6^+$, $Q_{EC} = 5000(9)$ keV [1]) the

*m.h.brunet@surrey.ac.uk

observed states are restricted to low to medium energy ($<Q_{EC}$) and single-digit-spin states by virtue of β-decay selection rules. Such restrictions offer an opportunity to observe these, predominantly nonyrast, states more exclusively than other production methods such as those used in a number of few-nucleon transfer reactions [2–4].

The EC/β^+ decay of ^{208}At populating ^{208}Po was last studied in the early 1980s [5,6]. The data produced were used to identify a large number of states and transitions in ^{208}Po, which were subsequently incorporated into a detailed decay scheme. The small Ge(Li) detectors used in these experiments had a lower efficiency than their modern counterparts, particularly at higher energies, thus many of the observed transitions remained unplaced [5,7–9].

Here we present results from an experiment performed at the ISOLDE Decay Station (IDS) at CERN. The high statistics provided by the increased detection efficiency of the large germanium detectors provided an opportunity to expand and improve upon previous works. Furthermore, it allowed for a more extensive study of the ^{208}At decay itself. The β population strength of states in ^{208}Po has been reported in previous work, but the higher detection efficiency allows for a better understanding of the population of high-energy states within the level scheme. These are often of negative parity and, therefore, populated in first-forbidden β decays.

II. EXPERIMENTAL DETAILS

The experiment was performed at the CERN-ISOLDE facility with the intention of measuring decays of ^{208}Hg [$T_{1/2}$ = 135(10) s] [10]. However, the beam contained an unexpectedly high yield of ^{208}At at $\approx 5 \times 10^4$ pps. Thus the data collected were used to investigate the β population of ^{208}Po.

To generate the desired beam, a molten lead target in conjunction with a VD5 FEBIAD [11] ion source was bombarded by a 1.4-GeV pulsed beam from the PS-Booster [12]. The proton beam intensity was ≈ 0.5 μA and the measurement lasted 7.5 h. A beam with mass $A = 208$ was extracted with a potential of 50 kV and mass separated using the General Purpose Separator. The cause of the abundance of ^{208}At is as yet unknown.

At the IDS, the beam was stopped on a movable tape, such that long-lived isotopes in the decay chains could be removed from the measurement area to avoid contaminating the desired spectrum. The tape cycle was set for a 539-s period of implantation followed by a further 539 s without implantation, after which the tape was moved. The four resident, four-crystal HPGe clover detectors at the IDS were combined with a fifth TIGRESS germanium detector [13], which provided a total γ efficiency of 11% at 100 keV and 4% at 1 MeV. The efficiency calibration was performed using ^{152}Eu and ^{60}Co sources. Extension of this up to an energy of 2615 keV utilized the known ratio [14] between the intensity of the 583-keV and that of the 2615-keV transition in ^{208}Pb following β decay of ^{208}Tl. A plastic scintillator block and photomultiplier tube setup surrounding the tape were used for β coincidence measurements. However, as ^{208}At predominantly decays via electron capture such coincidences are significantly less efficient and thus had little impact on this analysis. The triggerless total data readout system [15] at the IDS was used for data acquisition. More details are given in Refs. [16,17].

III. RESULTS

The predominantly β-decaying ground state of ^{208}At has spin parity 6^+ [14]. Due to γ and β selection rules, the ^{208}Po 0^+ ground state cannot be populated in a single γ transition. Therefore the data gathered in this experiment were used to generate matrices of $\gamma\gamma$ and $\beta\gamma\gamma$ coincidences from which the level scheme of ^{208}Po was built. Furthermore, due to the large spin change between parent and daughter ground states, a γ-normalization factor of 1.0 can be used to obtain photon intensities per 100 β^+/EC decays. Due to the presence of a long-lived isomeric state in ^{208}Po at 1528 keV [14], a coincidence window of 1 μs was selected to avoid significant loss of statistics in the coincidence spectra. The half-life of this isomeric state was determined in this analysis using time differences in coincidence spectra. A value of 377(9) ns was obtained as presented in [18], which is in agreement with the previously accepted value of 350(20) ns [14].

The full projection of the γ-γ matrix is presented in Fig. 1. This spectrum is dominated by transitions in ^{208}Po, populated from the β decay of ^{208}At [14]. The high detection efficiency of the large HPGe cluster detectors in place at the IDS results in higher statistics ($\approx 10^3$) than in previous experiments, particularly for higher-energy γ rays. As a consequence, Fig. 1 features a number of high-energy γ rays which were previously observed [14] but are not placed in the ^{208}Po level scheme.

As is typical for spectra of this nature two strong background peaks, 1460.8 and 2614.5 keV, which correspond to the decay of ^{40}K and ^{208}Tl, respectively [19], are clearly visible. In addition, a number of contaminant peaks result from $A = 207$ nuclei which were not fully removed by the mass separator. The most abundant of these is ^{207}Po, which EC/β^+ decays to ^{207}Bi. This decay can be attributed to all of the remaining labeled contaminant peaks (405.8, 742.7, 911.8, 1148.5, 1372.5, and 2060.8 keV [20]). Weaker γ rays from decays of ^{207,208}Tl and ^{207}Bi were also identified in energy-gated spectra but are not abundant enough to be visible in the full projection. Energy-gated spectra for transitions of interest are shown in [17,18].

The level scheme obtained for ^{208}Po populated via β^+/EC decay of ^{208}At is shown in Fig. 2. The full list of the observed transitions ranging in relative intensity from 0.01% to 100%, together with their properties, is given in Table I.The intensities were obtained from analysis of γ singles and γ-γ data, without the requirement for β-particle detection. The majority of the previously reported states populated in β decay [14] are confirmed, however, the previously suggested 3145-, 3202-, 3535-, and 4509-keV states were not observed and thus do not feature in the presented level scheme (note that the new 4508-keV state is based on different γ rays than the previous 4509-keV level). In addition, 27 new excited states and 43 new γ-ray transitions were observed for the first time. Furthermore, 33 of the previously observed but unplaced transitions are firmly included in the level scheme, which accounts for $\approx$45% of all previously unplaced transitions, including all

TABLE I. Full list of levels and transitions observed in ^{208}Po in this analysis. New states are indicated in boldface. New, assigned, and (re)assigned γ rays are indicated by x, y, and z superscripts, respectively. $E_{i/f}$ and $J^{\pi}_{i/f}$ are the energies and spin parities of initial and final states. E_{γ} is the measured energy of the transition. Multipolarities, where possible, have been taken from Ref. [14] and are based on previous conversion electron coefficient measurements from Refs. [5], [7], and [21]. When spin parities are not firmly established from experimental considerations, the assignment favored by shell model calculations is listed in boldface. References to Nuclear Data Sheet compilations [14] are provided for the spin parities of states which have been observed in non-β-decay studies. For instances where levels have only been observed previously in β-decay studies, all information relevant to their spin-parity assignments is provided here. I_{γ}, rel. and I_{γ} + IC, rel. represent the relative intensity of γ rays with and without internal electron conversion, with respect to 100 for the combined intensities of γs to the ground state (with IC). logft values were calculated using the measured transition intensity imbalances (given above the logft values as I_{β}% or the β population intensity per 100 decays). The Comment column lists additional information needed for the spin-parity assignments. *Note*: [x]The γ ray has been newly identified in this analysis. [y]The γ ray was observed in previous decay studies [14] and has been placed in the level scheme in this analysis. [z]The γ ray has been reassigned from its position in a prior analysis [14]. [*]The measured conversion coefficient was taken from [14], however, the multipolarity was reinterpreted from this analysis

E_i (keV)	J^{π}_i	E_f (keV)	J^{π}_f	E_{γ} (keV)	σL	$I_{\gamma,\text{rel.}}$	$I_{\gamma+\text{IC,rel.}}$	I_{β}% (logft)	Comment
686.6(2)	2^+ [14]	0.0	0^+	686.6(2)	E2 [14]	98(10)	100(10)	–	–
1263.2(3)	2^+ [14]	686.6(2)	2^+	576.7(3)	M1(+E2) [14]	0.35(9)	0.38(9)	–	–
		0.0	0^+	1263.0(2)	E2 [14]	0.15(1)	0.15(1)		
1346.7(3)	4^+ [14]	686.6(2)	2^+	660.1(2)	E2 [14]	92(8)	93(8)	–	–
1420.3(3)	3^+ [14]	686.6(2)	2^+	733.7(3)	M1 + E2 [14]	1.4(3)	1.4(3)	–	–
1524.4(3)	6^+ [14]	1346.7(3)	4^+	177.7(2)	E2 [14]	50(3)	87(4)	–	–
1528.3(5)	8^+ [14]	1524.4(3)	6^+	3.9(4)[a]	E2 [48,49]	–	40(2)[a]	–	–
1583.4(3)	4^+ [14]	1420.3(3)	3^+	163.3(3)	–	0.16(4)	0.46(21)	–	–
		1346.7(3)	4^+	236.8(2)	M1(+E2) [14]	0.35(5)	0.69(10)		
		686.6(2)	2^+	896.6(2)	E2 [14]	4.8(2)	4.8(2)		
1995.2(4)	3^-	1420.3(3)	3^+	575.3(3)	–	0.40(7)	0.41(8)	–	Populated by 3554- and 3610-keV 5^- states
		686.6(2)	2^+	1308.2(2)	E1(+M2) [14]	0.22(1)	0.22(1)		
2041.6(4)	6^+ [14]	1524.4(3)	6^+	517.2(2)	M1(+E2) [14]	6.3(4)	7.0(4)	3.8(12) 7.75(1)	Populated by M1 [14] 294-keV transition from 2336-keV 7^+ state
		1346.7(3)	4^+	[z]694.8(3)	–	2.5(4)	2.5(4)		
2149.1(4)	3^+, **4^+**	1583.4(3)	4^+	566.1(2)	M1 + E2 [14]	0.75(3)	0.80(4)	See text	–
		1420.3(3)	3^+	[z]729.2(3)	–	0.38(6)	0.39(6)		
		1346.7(3)	4^+	802.6(2)	–	0.40(6)	0.42(6)		
		686.6(2)	2^+	[x]1461.5(3)	–	0.57(5)	0.57(5)		
2160.3(5)	8^+ [14]	1528.3(5)	8^+	631.9(2)	M1(+E2) [14]	3.7(4)	3.9(4)	See text	–
2222.6(4)	8^+	2160.3(5)	8^+	[x]62.3(9)[a]	–	–	0.45(34)[a]	–	See text
		1528.3(5)	8^+	[z]694.3(2)	M1*	1.9(2)	2.0(2)		
		1524.4(3)	6^+	[z]698.2(2)	E2 [14]	1.24(7)	1.27(9)		
2280.8(3)	5^+	1346.7(3)	4^+	934.1(2)	M1 + E2 [14]	0.95(6)	0.97(6)	0.86(13) 8.32(7)	Populated by 3113-keV 5^-, 6^- state, J^{π} values limited by β^+ population
2293.8(4)	6^+ [14]	2041.6(4)	6^+	252.5(2)	–	0.62(6)	0.93(24)	4.13(57) 7.63(6)	–
		1583.4(3)	4^+	710.5(2)	–	0.65(2)	0.66(2)		
		1528.3(5)	8^+	765.2(3)	–	0.13(7)	0.14(7)		
		1524.4(3)	6^+	769.5(2)	M1(+E2) [14]	2.1(2)	2.2(2)		
		1346.7(3)	4^+	947.0(2)	E2 [14]	1.60(4)	1.61(4)		
2335.7(5)	7^+ [14]	2041.6(4)	6^+	294.2(2)	M1 [14]	0.99(7)	1.53(11)	6.50(49) 7.42(4)	–
		1528.3(5)	8^+	807.2(2)	M1(+E2) [14]	6.2(2)	6.4(2)		
		1524.4(3)	6^+	811.4(2)	M1 +E2 [14]	1.22(7)	1.25(7)		
2369.3(4)	7^- [14]	1528.3(5)	8^+	840.8(4)	E1 [14]	3.0(3)	3.0(3)	–	–
		1524.4(3)	6^+	845.1(2)	E1 [14]	21.1(7)	21.1(7)		

TABLE I. *(Continued).*

E_i (keV)	J_i^π	E_f (keV)	J_f^π	E_γ (keV)	σL	$I_{\gamma,\text{rel.}}$	$I_{\gamma+\text{IC,rel.}}$	I_β% (log*ft*)	Comment
2402.1(5)	$3^-, 4^+$	1263.2(3)	2^+	[y]1139.0(4)	E1,E2 [14]	0.5(2)	0.5(2)	–	Populated by 3610-keV 5^- state and 3683-keV $5^-, 6^-$ state
2415.0(5)	$\mathbf{7}^+, 8^+$	2160.3(5)	8^+	254.8(3)	–	0.32(4)	0.48(14)	–	Populated by 3565-keV 6^- state
		2041.6(4)	6^+	373.4(2)	–	0.71(4)	0.80(12)		
		1528.3(5)	8^+	886.3(2)	M1 + E2 [14]	2.95(9)	3.02(9)		
		1524.4(3)	6^+	[x]890.8(3)	–	0.47(4)	0.47(4)		
2437.6(4)	5^+	1420.3(3)	3^+	[y]1017.2(2)	E2*	0.77(6)	0.78(6)	–	See text
2507.7(3)	$5^+, \mathbf{6}^+$	2293.8(4)	6^+	214.1(3)	M1 +E2 [14]	0.28(5)	0.59(12)	5.91(20) 7.39(2)	–
		1583.4(3)	4^+	[z]924.2(2)	–	0.57(5)	0.58(6)		
		1524.4(3)	6^+	983.2(2)	M1 + E2 [14]	4.7(2)	4.7(2)		
2526.7(4)	5^+	2041.6(4)	6^+	485.0(2)	M1 [14]	0.44(5)	0.50(6)	1.74(21) 7.92(6)	–
		1524.4(3)	6^+	1002.2(2)	M1(+E2) [14]	0.45(2)	0.46(2)		
		1420.3(3)	3^+	[x]1106.9(3)	–	0.30(3)	0.30(3)		
		1346.7(3)	4^+	1179.6(2)	M1(+E2) [14]	1.05(4)	1.05(4)		
2556.5(5)	7^+ [14]	2369.3(4)	7^-	[y]188.2(2)	–	0.5(2)	0.5(2)	22.9(16) 6.8(2)	–
		2293.8(4)	6^+	262.0(3)	M1(+E2) [14]	0.38(6)	0.62(13)		
		2222.6(4)	8^+	[z]333.9(3)	M1(+E2) [14]	2.5(5)	2.9(9)		
		2160.3(5)	8^+	396.2(3)	M1 + E2 [14]	1.16(2)	1.41(4)		
		1528.3(5)	8^+	1027.7(2)	M1 + E2 [14]	19.4(7)	19.7(7)		
2574.8(4)	$\mathbf{6}^-, 7^-$ [14]	2369.3(4)	7^-	205.5(2)	M1(+E2) [14]	7.9(4)	19.4(9)	–	–
		1524.4(3)	6^+	[x]1050.3(2)	–	0.26(3)	0.26(3)		
2863.0(4)	$3^-, 4, 5, 6^+$	2402.1(5)	$3^-, 4^+$	[x]460.9(3)	–	0.23(7)	0.24(8)	–	Populated by 3553- and 3610-keV 5^- states
		1583.4(3)	4^+	[y]1279.62(2)	–	0.87(7)	0.87(7)		
2884.5(3)	5^-	1583.4(3)	4^+	[z]1301.2(3)	–	0.12(3)	0.12(3)	–	–
		1524.4(3)	6^+	1360.0(2)	E1 [14]	0.99(1)	0.99(1)		
		1346.7(3)	4^+	1537.6(2)	E1 [14]	1.52(5)	1.52(5)		
2926.6(4)	5^-	2574.8(4)	$6^-, 7^-$	[x]351.7(4)	–	0.31(7)	0.35(11)	0.62(47) 8.2(4)	M1 + E2 [14] (638-keV) transition from 3565-keV 6^- state
		1583.4(3)	4^+	1343.4(2)	E1 [14]	2.46(8)	2.46(8)		
		1346.7(3)	4^+	[x]1579.9(4)	–	0.4(2)	0.4(2)		
3024.2(5)	$6^+, 7, 8^-$	2222.6(4)	8^+	[x]801.6(3)	–	0.48(8)	0.48(9)	0.91(13) 8.0(2)	J^π values limited by β^+ population
		2160.3(5)	8^+	[y]863.8(2)	–	0.42(4)	0.42(4)		
3072.5(4)	$6^-, 7^-, 8^-$	2041.6(4)	6^+	[x]1030.9(3)	–	0.32(5)	0.32(5)	–	M1(+E2) [14] transition from 4167-keV 7^- state
3103.8(4)	$4^-, 5, 6, 7, 8^-$	2041.6(4)	6^+	[y]1062.2(3)	–	0.10(3)	0.10(3)	0.10(3) 8.9(2)	J^π values limited by β^+ population
3113.3(5)	$5^-, 6^-$	2574.8(4)	$6^-, 7^-$	538.6(3)	M1 + E2 [14]	0.30(7)	0.32(7)	–	–
		2369.3(4)	7^-	[x]744.0(3)	–	0.26(7)	0.27(7)		
		2280.8(3)	5^+	[z]832.6(7)	–	0.06(6)	0.06(6)		
		2041.6(4)	6^+	1071.4(3)	–	0.25(4)	0.25(4)		
		1524.4(3)	6^+	1588.8(2)	–	0.24(1)	0.24(1)		
3163.7(5)	$4^-, 5^-, 6^-$	2574.8(4)	$6^-, 7^-$	[x]588.9(4)	–	0.6(2)	0.6(2)	–	M1(+E2) [14] from 3554-keV 5^- state
		1583.4(3)	4^+	[y]1580.3(4)	–	0.31(8)	0.31(8)		
3276.0(5)	$4^-, 5, 6, 7^-$	2884.5(3)	5^-	[x]391.6(3)	–	0.14(4)	0.16(5)	–	See text
		2149.1(4)	$3^+, 4^+$	[x]1126.2(5)	–	0.24(8)	0.24(8)		
		1583.4(3)	4^+	[y]1692.8(3)	–	0.32(5)	0.32(5)		

TABLE I. *(Continued).*

E_i (keV)	J_i^π	E_f (keV)	J_f^π	E_γ (keV)	σL	$I_{\gamma,\mathrm{rel.}}$	$I_{\gamma+\mathrm{IC,rel.}}$	I_β% (log*ft*)	Comment
		1346.7(3)	4^+	[y]1929.8(4)	–	0.20(4)	0.20(4)		
3441.8(5)	$4^-, 5^-, 6^+$	2926.6(4)	5^-	[x]515.5(4)	–	0.33(5)	0.35(7)	0.65(9) 7.9(7)	J^π values limited by β^+ population
		1346.7(3)	4^+	[z]2094.8(2)	E1,E2 [14]	0.30(4)	0.30(4)		
3533.6(4)	$5^-, 6^-, 7^-$	2926.6(4)	5^-	[x]606.7(3)	–	0.12(3)	0.12(3)	1.39(20) 7.52(7)	–
		2884.5(3)	5^-	[x]649.4(3)	–	0.17(3)	0.18(4)		
		2574.8(4)	$6^-, 7^-$	[y]958.9(2)	M1(+E2) [14]	0.71(8)	0.73(9)		
		2369.3(4)	7^-	[y]1164.2(3)	–	0.37(6)	0.37(6)		
3553.9(4)	5^-	3276.0(5)	$4^-, 5, 6, 7^-$	[x]278.5(4)	–	0.15(7)	0.19(11)	5.31(60) 6.94(6)	–
		3163.7(5)	$4^-, 5^-, 6^-$	[z]390.3(2)	M1(+E2) [14]	0.48(9)	0.53(13)		
		2926.6(4)	5^-	627.1(2)	M1(+E2) [14]	0.29(4)	0.31(4)		
		2884.5(3)	5^-	669.5(2)	M1(+E2) [14]	1.32(3)	1.38(5)		
		2863.0(4)	$3^-, 4, 5, 6^+$	[x]691.2(1)	–	0.34(2)	0.34(3)		
		2149.1(4)	$3^+, 4^+$	[x]1404.6(4)	–	0.24(6)	0.24(6)		
		2041.6(4)	6^+	[z]1512.4(3)	E1 [14]	0.24(3)	0.24(3)		
		1995.2(4)	3^-	[x]1558.2(5)	–	0.3(2)	0.3(2)		
		1583.4(3)	4^+	1970.3(2)	–	0.12(1)	0.12(1)		
		1524.4(3)	6^+	2029.4(2)	E1 [14]	1.30(6)	1.30(6)		
		1346.7(3)	4^+	2207.0(2)	E1 [14]	0.41(3)	0.41(3)		
3564.8(4)	6^-	3276.0(5)	$4^-, 5, 6, 7^-$	[x]289.6(10)	–	0.1(1)	0.1(1)	25.9(15) 6.24(1)	–
		3113.3(5)	$5^-, 6^-$	451.7(4)	M1(+E2) [14]	0.6(3)	0.7(3)		
		2926.6(4)	5^-	[z]638.1(2)	M1 + E2 [14]	0.34(4)	0.35(5)		
		2574.8(4)	$6^-, 7^-$	990.0(2)	M1(+E2) [14]	16.3(5)	16.6(5)		
		2556.5(5)	7^+	1008.6(2)	E1 [14]	1.92(6)	1.92(6)		
		2526.7(4)	5^+	1038.1(3)	(E1 + M2) [14]	0.52(3)	0.52(3)		
		2437.6(4)	5^+	[z]1126.9(4)	E1*	0.12(5)	0.12(5)		
		2415.0(5)	$7^+, 8^+$	[x]1149.5(3)	–	1.2(3)	1.2(3)		
		2369.3(4)	7^-	1195.2(2)	M1 + E2 [14]	1.86(4)	1.86(4)		
		2335.7(5)	7^+	1229.1(2)	E1 [14]	2.5(2)	2.5(2)		
		2041.6(4)	6^+	1523.5(3)	–	0.07(2)	0.07(2)		
3610.1(4)	5^-	3276.0(5)	$4^-, 5, 6, 7^-$	[x]334.1(7)	–	0.2(2)	0.3(2)	3.28(43) 7.10(6)	–
		2863.0(4)	$3^-, 4, 5, 6^+$	[y]747.4(1)	–	0.62(6)	0.63(7)		
		2402.1(5)	$3^-, 4^+$	[x]1208.3(2)	–	0.21(3)	0.21(3)		
		2149.1(4)	$3^+, 4^+$	[x]1460.6(2)	–	0.70(6)	0.70(6)		
		1995.2(4)	3^-	[x]1614.4(3)	–	0.37(9)	0.37(9)		
		1583.4(3)	4^+	[y]2026.7(2)	E1*	0.61(4)	0.61(4)		
		1524.4(3)	6^+	[y]2085.9(2)	E1 [14]	0.55(4)	0.55(4)		
3682.6(4)	$5^-, 6^-$	3276.0(5)	$4^-, 5, 6, 7^-$	[x]406.5(3)	–	0.4(2)	0.5(2)	4.46(64) 6.91(7)	–
		3163.7(5)	$4^-, 5^-, 6^-$	[x]518.9(4)	–	0.4(2)	0.5(2)		
		2926.6(4)	5^-	755.5(2)	M1(+E2) [14]	1.30(2)	1.35(2)		
		2884.5(3)	5^-	798.2(2)	M1(+E2) [14]	0.75(6)	0.78(6)		
		2863.0(4)	$3^-, 4, 5, 6^+$	[x]820.0(4)	–	0.15(4)	0.15(4)		
		2574.8(4)	$6^-, 7^-$	1107.9(3)	M1 + E2 [14]	0.54(8)	0.54(8)		
		2402.1(5)	$3^-, 4^+$	[z]1281.7(3)	–	0.19(3)	0.19(3)		
		2041.6(4)	6^+	1640.6(5)	E1 [14]	0.12(4)	0.12(4)		
		1524.4(3)	6^+	2157.8(6)	–	0.14(5)	0.14(5)		
		1346.7(3)	4^+	2336.0(3)	–	0.38(4)	0.38(4)		
3708.0(5)	$5^-, 6^-, 7^-, 8^-$	2574.8(4)	$6^-, 7^-$	[y]1133.2(4)	M1 + E2 [14]	0.36(10)	0.36(10)	0.36(10) 8.0(2)	–
3744.5(5)	$5^-, 6, 7, 8^-$	2160.3(5)	8^+	[z]1584.2(2)	–	0.07(1)	0.07(1)	0.07(1) 8.67(7)	J^π values limited by β^+ population
3808.4(4)	$6^-, 7^-$	2574.8(4)	$6^-, 7^-$	1233.9(3)	–	0.42(6)	0.42(6)	1.80(16) 7.21(5)	J^π values limited by β^+ population and logft
		2369.3(4)	7^-	1438.9(2)	M1 + E2 [14]	1.26(7)	1.26(7)		
		2335.7(5)	7^+	1472.7(6)	–	0.03(2)	0.03(2)		
		1524.4(3)	6^+	2283.8(3)	–	0.10(2)	0.10(2)		

TABLE I. *(Continued).*

E_i (keV)	J_i^π	E_f (keV)	J_f^π	E_γ (keV)	σL	$I_{\gamma,\text{rel.}}$	$I_{\gamma+\text{IC,rel.}}$	I_β% (logft)	Comment
3893.9(4)	$4^-, 5, 6, 7^-$	2926.6(4)	5^-	[x]967.0(4)	–	0.03(2)	0.03(2)	0.79(16) 7.5(1)	J^π values limited by β^+ population
		2437.6(4)	5^+	[y]1456.3(4)	–	0.4(2)	0.4(2)		
		2280.8(3)	5^+	[y]1613.2(3)	–	0.03(1)	0.03(1)		
		1524.4(3)	6^+	[y]2369.8(2)	–	0.36(2)	0.36(2)		
3904.3(6)	$4^-, 5, 6, 7, 8^-$	2556.5(5)	7^+	[x]1346.7(2)	–	0.28(2)	0.28(2)	0.37(12) 7.8(2)	–
		2437.6(4)	5^+	[y]1467.9(10)	–	0.08(4)	0.08(4)		
4018.9(5)	5,6,7	3113.3(5)	$5^-, 6^-$	[x]905.2(4)	–	0.5(3)	0.6(3)	1.35(28) 7.17(9)	J^π values limited by β^+ population and logft
		2526.7(4)	5^+	[x]1492.8(8)	–	0.05(4)	0.05(4)		
		2293.8(4)	6^+	1725.0(2)	–	0.02(1)	0.02(1)		
		1524.4(3)	6^+	2494.6(2)	–	0.73(3)	0.73(3)		
4046.8(5)	$4^-, 5, 6, 7, 8^-$	2335.7(5)	7^+	[x]1710.8(4)	–	0.03(1)	0.03(1)	0.15(4) 8.1(2)	J^π values limited by β^+ population
		1524.4(3)	6^+	[y]2522.8(4)	–	0.12(3)	0.12(3)		
4079.4(4)	5,6,7	2574.8(4)	$6^-, 7^-$	[x]1504.8(3)	–	0.35(6)	0.35(6)	0.64(10) 7.41(8)	J^π values limited by β^+ population and logft
		2280.8(3)	5^+	[x]1798.3(4)	–	0.02(1)	0.02(1)		
		2041.6(4)	6^+	[y]2037.8(2)	–	0.15(1)	0.15(1)		
		1524.4(3)	6^+	[y]2555.2(4)	–	0.12(2)	0.12(2)		
4143.2(5)	5,6,7	2415.0(5)	$7^+, 8^+$	[x]1728.0(3)	–	1.8(3)	1.8(3)	2.38(33) 6.77(7)	J^π values limited by β^+ population and logft
		2369.3(4)	7^-	[y]1773.5(3)	–	0.34(4)	0.34(4)		
		2335.7(5)	7^+	[x]1807.9(4)	–	0.03(1)	0.03(1)		
		2041.6(4)	6^+	[y]2101.3(3)	–	0.04(1)	0.04(1)		
		1524.4(3)	6^+	[y]2619.3(4)	–	0.21(3)	0.21(3)		
4166.6(5)	7^-	3072.5(4)	$6^-, 7^-, 8^-$	[y]1094.4(3)	M1(+E2) [14]	0.32(5)	0.32(5)	5.43(81) 6.39(8)	–
		2415.0(5)	$7^+, 8^+$	1751.7(4)	E1 [14]	1.5(5)	1.5(5)		
		2369.3(4)	7^-	1796.9(2)	M1(+E2) [14]	0.69(1)	0.69(1)		
		2335.7(5)	7^+	1830.4(4)	–	0.03(1)	0.03(1)		
		2293.8(4)	6^+	1872.6(3)	E1 [14]	0.19(3)	0.19(3)		
		2222.6(4)	8^+	[y]1944.1(3)	–	0.12(3)	0.12(3)		
		2041.6(4)	6^+	2125.1(3)	E1 [14]	0.46(5)	0.46(5)		
		1528.3(5)	8^+	2638.5(3)	–	1.70(9)	1.70(9)		
		1524.4(3)	6^+	2642.4(5)	–	0.47(4)	0.47(4)		
4187.2(4)	$4^-, 5, 6, 7, 8^-$	1524.4(3)	6^+	[y]2662.7(3)	–	0.04(1)	0.04(1)	0.04(1) 8.5(2)	J^π values limited by β^+ population
4196.0(7)	$5^-, 6, 7, 8^-$	1528.3(5)	8^+	[z]2667.7(5)	–	0.04(1)	0.04(1)	0.04(1) 8.5(2)	J^π values limited by β^+ population
4209.1(4)	$5^+, 6^+, 7^+$	2437.6(4)	5^+	[x]1772.5(4)	–	0.10(2)	0.10(2)	0.31(4) 7.58(7)	J^π values limited by β^+ population
		2041.6(4)	6^+	[y]2168.2(2)	E2,M1 [14]	0.21(1)	0.21(1)		
4251(1)	$4^-, 5, 6, 7, 8^-$	2574.8(4)	$6^-, 7^-$	[x]1675.8(5)	–	0.15(6)	0.15(6)	0.19(8) 7.7(2)	J^π values limited by β^+ population
		2335.7(5)	7^+	1916.8(3)	–	0.04(2)	0.04(2)		
4257.1(4)	$4^-, 5, 6, 7, 8^-$	1524.4(3)	6^+	[y]2732.7(3)	–	0.09(1)	0.09(1)	0.09(1) 8.05(6)	J^π values limited by β^+ population
4426.9(6)	$5, 6, 7, 8^-$	2369.3(4)	7^-	[x]2057.4(6)	–	0.03(1)	0.03(1)	0.07(3) 7.9(2)	J^π values limited by β^+ population
		2335.7(5)	7^+	[z]2091.3(6)	–	0.01(1)	0.01(1)		
		1524.4(3)	6^+	[y]2902.6(4)	–	0.03(1)	0.03(1)		
4468.3(7)	$4^-, 5, 6, 7, 8^-$	2437.6(4)	5^+	[x]2030.8(6)	–	0.10(5)	0.10(5)	0.10(5) 7.7(3)	J^π values limited by β^+ population

TABLE I. *(Continued).*

E_i (keV)	J_i^π	E_f (keV)	J_f^π	E_γ (keV)	σL	$I_{\gamma,\text{rel.}}$	$I_{\gamma+\text{IC,rel.}}$	I_β% (logft)	Comment
4508.2(5)	$4^-, 5, 6, 7$	2926.6(4)	5^-	[y]1581.5(4)	–	0.08(2)	0.08(2)	0.08(2) 7.7(2)	J^π values limited by β^+ population
4524.9(6)	$4^-, 5, 6, 7, 8^-$	1524.4(3)	6^+	[y]3000.5(5)	–	0.03(1)	0.03(1)	0.03(1) 8.1(2)	J^π values limited by β^+ population

[a]This low-energy γ ray was not observed directly. Its energy and intensity were determined from coincidence relationships.

those with a relative intensity greater than 0.35% [14] (a more detailed analysis is given in Ref. [17]). In addition, 17 γ-ray placements were changed from a previous analysis based on coincidence relationships observed, however, most were of a relatively low intensity.

The spin-parity assignments of the excited states are based on their decay pattern and on previously reported experimental information and occasionally are restricted by experimentally determined logft values. Realistically, only E1, M1, and E2 transitions can occur however, M2 and E3 transitions were considered for high energies ($E_\gamma > 1$ MeV), the latter of which is justified by the strong octupole collectivity in the region. Internal conversion coefficients were previously measured for a large number of transitions, sometimes even for transitions which were not placed in the level scheme [5,7,21]. These often proved to be crucial for our spin-parity assignments. The logft values were determined from measured γ-ray intensities and used to limit spin-parity values of β-populated states based on comparison with recommended ranges [22], where the lower limit for first-forbidden unique decays ($\Delta J = 2$, $\Delta\pi =$ yes) is 7.5. Internal electron conversion was considered. If no experimental value was available, theoretical internal conversion coefficients were used from the BrIcc code [23]. When the multipolarity was unknown an average internal conversion coefficient value was used with sufficient uncertainty to cover E1, M1, and E2 possibilities. The list of observed states, with justification of their spin-parity assignments, and logft values is given in Table I. Several states were previously populated in experiments involving different types of reactions and their spin parities were already unambiguously established. In this case we refer to the Nuclear Data Sheets evaluation [14]. A small number of

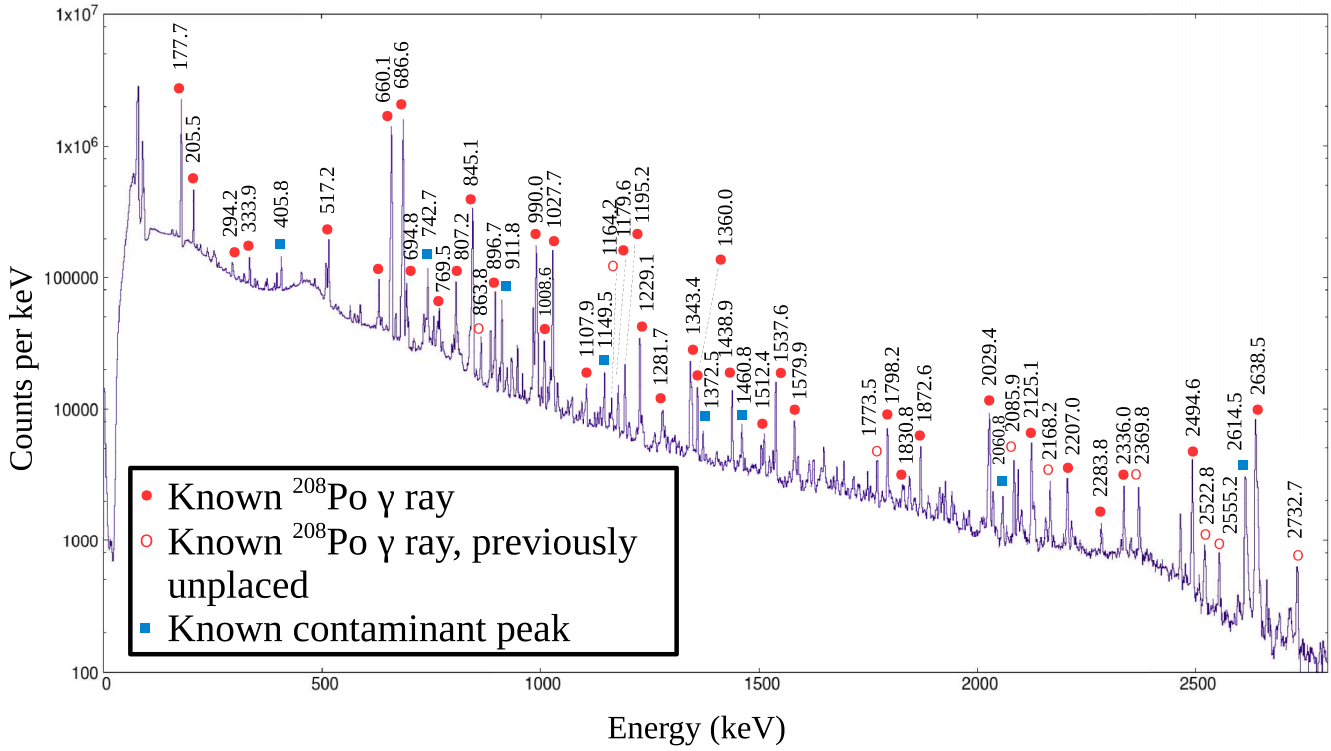

FIG. 1. Full γ-γ matrix projection (1-μs coincidence window) for all $A = 208$ data collected. Peak positions are given for previously identified ^{208}Po γ rays (indicated by filled red circles), known ^{208}Po but previously unplaced γ rays (indicated by open red circles), and known contaminant peaks (indicated by filled blue squares). The contaminant peaks feature results from decays in ^{207}Bi, as well as strong background peaks (^{40}K at 1460.8 keV and ^{208}Tl at 2614.5 keV).

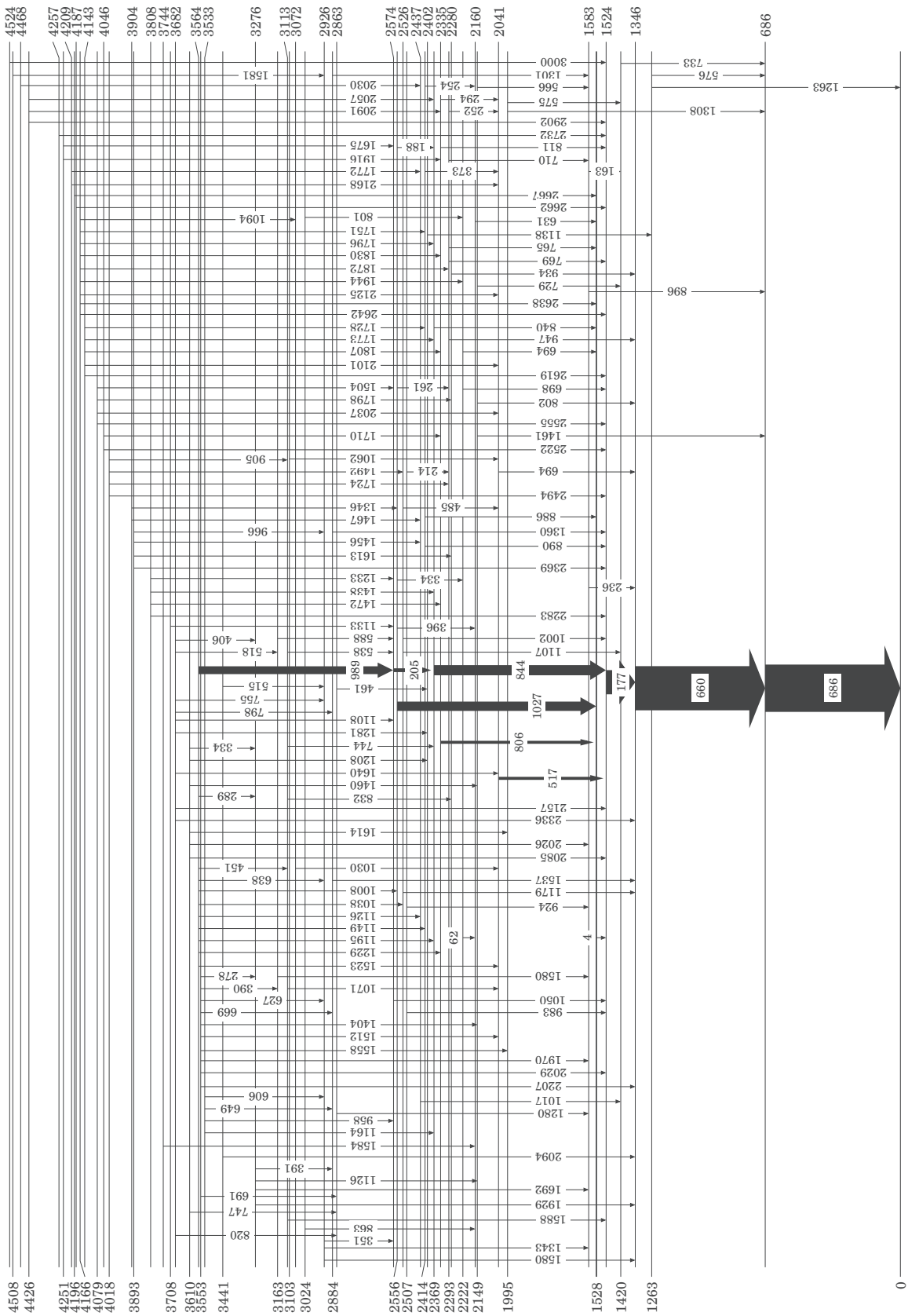

FIG. 2. Level scheme for ^{208}Po observed in this work. Energies of levels and transitions are given in keV. Relative intensities of the most intense transitions are indicated by the thicknesses of arrows.

states require additional explanation; the following paragraphs detail the justifications for the spin-parity assignments of these states.

The log*ft* values indicate that states which were fed directly were populated in either allowed or first-forbidden β decays. We note that according to our level scheme and transition intensities, the 2149-keV 3^+, 4^+ and the 2160-keV 8^+ states are populated directly by β decay at levels of 1.0(4)% and 1.1(5)%, respectively. These correspond to logft values around 8, much lower than previously observed for a second-forbidden decay [22]. These population intensities are roughly within two standard deviations from 0 and thus the logft values are not listed in Table I. In addition, some internal feeding into these states may not have been observed.

The 2223-keV level is the lowest-energy new state identified in the present work. Its spin parity is determined by the properties of its depopulating transitions as listed in Table I. Both of the observed transitions at energies of 694 and 698 keV, as well as the 334-keV transition directly populating the 2223-keV state, were observed previously, and their internal conversion coefficients measured. However, all were placed in different parts of the level scheme [14]. The multipolarities of the 698- and 334-keV transitions fix the spin parity of the 2223-keV level at 8^+. The 694-keV peak results from a doublet. The electron conversion coefficient $\alpha_K = 0.026(4)$ [5,7,14] was measured for the doublet and the multipolarity of the 694.8-keV transition from the 2042-keV 6^+ level has to be E2. Considering these factors the conversion coefficient of the 694.3-keV transition can be calculated as $\alpha_K = 0.05(1)$, indicating an M1 character, in agreement with the spin-parity assignment.

The 2438-keV state is populated, among others, by an 1126-keV transition from a 6^- state with a previously measured conversion coefficient of $\alpha_K \leqslant 0.006$ [21], which limits its multipolarity to E1 or E2. In addition, the 2438-keV state decays via a 1017-keV transition to a 3^+ state which was assigned M1 + E2 multipolarity on account of the internal conversion coefficient measurement of $\alpha_K = 0.010(2)$ [5]. Here we reinterpret it as either M1 ($\alpha_K = 0.016$) or E2 ($\alpha_K = 0.006$). This reinterpretation allows for an unmixed E2 character which fixes the spin parity of the 2438-keV level to 5^+.

The 3276-keV state decays, among others, by two previously identified but unplaced transitions at 1693 and 1930 keV [21], both populating firmly established 4^+ states. However, based on conversion coefficient measurements, the 1693-keV γ ray was identified as an E1 transition, while the 1930-keV γ ray was M1 + E2 [14,21]. These require opposite parities and are thus unresolvable. At this time we do not have a solution to this discrepancy.

IV. DISCUSSION

The experimental results were compared to shell model calculations to gain a better understanding of the structure of the observed states. The shell model calculations were performed with the NUSHELLX code [24]. The modified Kuo-Herling Hamiltonian [25] was used for the proton-proton and neutron-neutron interactions, with the M3Y potential [26,27] for the proton-neutron interaction. Single-particle energies were taken from Fig. 1 in [25]. The model space used considers the proton and neutron orbitals $1h_{9/2}$, $2f_{7/2}$, $2f_{5/2}$, $3p_{3/2}$, $3p_{1/2}$, and $1i_{13/2}$, covering $82 < Z$, $N < 126$. Therefore for ^{208}Po this gives two proton-particle and two neutron-hole states and no core excitations. For the E2 matrix elements radial wave functions from the Skx Skyrme Hartree-Fock calculation [28] were used. The effective charges were $e_p = 1.5e$ and $e_n = 0.8e$ for E2 transitions, taken from [29]. Free nucleon g factors were used for the M1 and M2 matrix elements ($g_{sp} = 5.586$ and $g_{sn} = -3.826$, with $g_{lp} = 1.0$, and $g_{ln} = 0.0$). The E1 matrix elements are 0 in this model space.

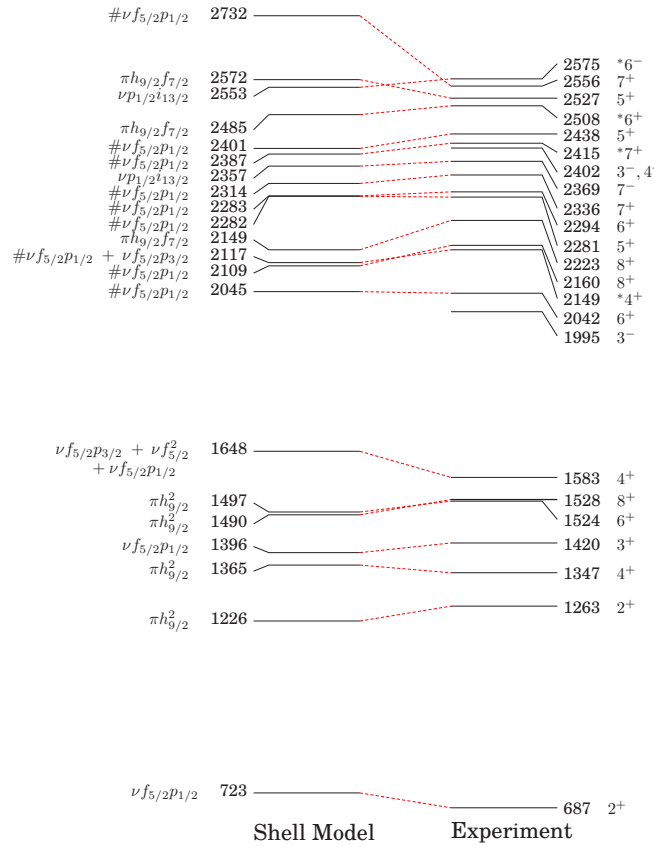

FIG. 3. Comparison of shell model and experimental excited states in ^{208}Po. Left: Dominant configurations are given, taken from shell model calculations, with # denoting $\pi h^2_{9/2}$. Right: Spin-parity assignments, with asterisks denoting states where assignments have been made using branching ratio comparisons.

The dominant configuration of the ^{208}Po ground state is $\pi(h^2_{9/2})\nu(p^{-2}_{1/2})$. The experimental level scheme is compared with predictions from the shell model in Fig. 3, with the dominant configurations indicated. The $\pi h^2_{9/2}$ seniority scheme is reproduced, however, the ordering of the 8^+ and 6^+ $\pi h^2_{9/2}$ states is inverted in the calculations. For several states no firm spin-parity assignment could be achieved based on experimental considerations. In most of these cases, indicated by asterisks in Fig. 3, a preferred spin parity could be proposed

TABLE II. Comparison between experimental and shell model γ-ray branching ratios. Only transitions with an experimental or theoretical $BR_\gamma > 1\%$ are listed. In some cases no firm experimental spin-parity assignments could be achieved, as shown in Table I. When the proposed spin parity is based on comparison with theory, it is preceded by a superscript asterisk.

Experiment			Shell model		
E_i (keV)/J_i^π	E_f (keV)/J_f^π	BR_γ (%)	E_i (keV)	E_f (keV)	BR_γ (%)
$687/2^+$	0	100	723	0	100
$1263/2^+$	$687/2^+$	70	1226	723	30
	$0/0^+$	30		0	70
$1347/4^+$	$687/2^+$	100	1365	723	100
$1420/3^+$	$1263/2^+$	–	1396	1226	1
	$687/2^+$	100		723	99
$1524/6^+$	$1347/4^+$	100	1497	1365	100
$1528/8^+$	$1524/6^+$	100	1490	–	-[a]
$1583/4^+$	$1420/3^+$	3	1648	1396	13
	$1347/4^+$	7		1365	4
	$687/2^+$	90		723	83
$2042/6^+$	$1524/6^+$	72	2045	1497	61
	$1347/4^+$	28		1365	38
$2149/*4^+$	$1583/4^+$	36	2117	1648	26
	$1420/3^+$	18		1396	59
	$1347/4^+$	19		1365	8
	$687/2^+$	27		723	7
$2160/8^+$	$1528/8^+$	100	2109	1490	99
	$1524/6^+$	–		1497	1
$2223/8^+$	$2160/8^+$	≈1	2149	2109	1
	$1524/6^+$	39		1497	70
	$1528/8^+$	61		1490	29
$2281/5^+$	$2042/6^+$	–	2282	2045	6
	$1583/4^+$	–		1648	3
	$1524/6^+$	–		1497	15
	$1347/4^+$	100		1365	75
$2294/6^+$	$2042/6^+$	12	2283	2045	11
	$1583/4^+$	13		1648	10
	$1524/6^+$	41		1497	38
	$1528/8^+$	3		1490	1
	$1347/4^+$	31		1365	41
$2336/7^+$	$2160 / 8^+$	–	2314	2109	1
	$2042/6^+$	12		2045	14
	$1524/6^+$	15		1497	21
	$1528/8^+$	74		1490	64
$2369/7^-$	$1528/8^+$	12	2357	1490	0.3
	$1524/6^+$	88		1497	100
$2415/*7^+$	$2223/8^+$	–	2387	2149	4
	$2160/*8^+$	7		2109	6
	$2042/6^+$	16		2045	4
	$1524/6^+$	11		1497	7
	$1528/8^+$	66		1490	79
$2438/5^+$	$2042/6^+$	–	2401	2045	2
	$1583/4^+$	–		1648	3
	$1524/6^+$	–		1497	29
	$1420/3^+$	100		1396	61
	$1347/4^+$	–		1365	3
$2508/*6^+$	$2415/*7^+$	–	2485	2387	1
	$2336/7^+$	–		2314	1
	$2294/6^+$	5		2283	7
	$2281/*5^+$	–		2282	1
	$2042/6^+$	–		2045	3
	$1583/4^+$	10		1648	2
	$1524/6^+$	85		1497	83
	$1528/8^+$	–		1490	1
$2527/5^+$	$2294/6^+$	–	2572	2283	5
	$2281/*5^+$	–		2282	5
	$2149/*4^+$	–		2117	9
	$2042/6^+$	20		2045	23
	$-/4^+$	–		2005	4
	$1583/4^+$	–		1648	8
	$1524/6^+$	20		1497	30
	$1420/3^+$	13		1396	2
	$1347/4^+$	47		1365	13
$2556/7^+$	$2369/7^-$	2	2732[b]	2357	<1
	$2336/7^+$	–		2314	4
	$2294/6^+$	2		2283	<1
	$2223/8^+$	10		2149	45
	$2160/*8^+$	5		2109	3
	$2042/6^+$	–		2045	11
	$1524/6^+$	–		1497	5
	$1528/8^+$	81		1490	32
$2575/*6^-$	$2369/7^-$	97	2553	2357	100
	$1524/6^+$	3		1497	<1

[a]Due to the inversion of the 6^+ and 8^+ states, no branching ratio could be calculated, however, the theoretical B(E2) value (≈)1 W.u.) indicates the existence of a transition between the two states.

[b]There is a 7^+ state predicted at 2618 keV, which is closer to the experimental value. However, its decay pattern is very different from the observed one.

by comparing measured and theoretical branching ratios, as reported in Table II. However, this argument is weak and thus purely used for comparison with theoretical calculations. A firm or preferred spin parity was assigned for all levels up to 2.6-MeV excitation energy (excluding 2402 keV). A good agreement (usually within 100 keV) between experiment and shell model level energies was obtained for all these excited states. Shell model calculations using a smaller model space (neutron orbitals $2f_{5/2}$, $3p_{3/2}$, $3p_{1/2}$, $1i_{13/2}$ and proton orbitals $1h_{9/2}$, $2f_{7/2}$, $1i_{13/2}$) were compared in [18] to experimental results, which showed a greater energy disparity and systematic energy shift.

The only levels without theoretical counterparts are the 3^- state at 1995 keV and the 2402-keV level. The former is a collective octupole state and is thus not reproducible within the model space used. It is discussed in detail in Ref. [30].

The 2402-keV level has been assigned 3^- or 4^+ spin parity. There is a 4^+ state with a similar energy predicted by the shell model at 2473 keV, however, the decay pattern of this state does not match what was observed [17]. At the same time the closest 3^- state predicted in the present model space is at 2824 keV. Therefore we do not have a preferred spin-parity assignment for the 2402-keV level.

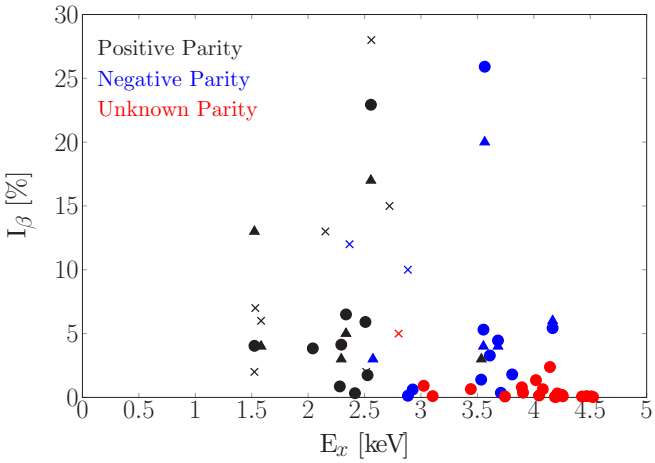

FIG. 4. β-population intensity as a function of the ^{208}Po excitation energy. The present results are indicated by filled circles. These are compared with result obtained from experiments performed in the 1960s [8] (x's) and the 1980s [14] (filled triangles). The parity of the excited states is indicated by the color of the symbol.

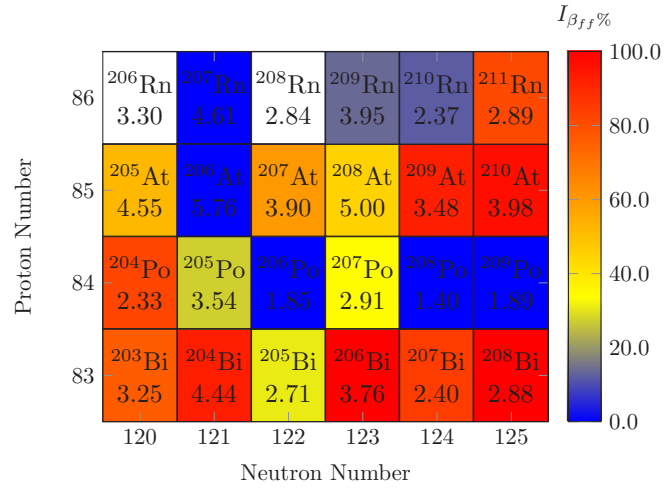

FIG. 5. Intensity of first-forbidden decays ($I_{\beta_{\rm ff}}\%$) for proton-rich A $\approx$ 208 nuclei [14,20,32–38]. $I_{\beta_{\rm ff}}\% = I_{\beta_{\rm ff}}/I_{\beta_{\rm tot}}$. The parent nuclei are indicated. $Q_{\rm EC}$ values, in MeV, are also given. In the majority of nuclei, competition between first-forbidden and allowed β decay is expected. For details, see the text.

V. BETA DECAY

Both positive- and negative-parity states are fed directly in the β^+/EC decay of ^{208}At. The β-decay feeding intensity as a function of the excited-state energy in ^{208}Po is shown in Fig. 4. According to the present work $\approx$44% of the decay proceeds via allowed β decay and $\approx$46% via first-forbidden decay, with the remaining $\approx$10% decaying to states of unknown parity.

The large role of first-forbidden decays can be qualitatively understood through shell model considerations. All allowed transitions are hindered. The decays populating non-core-excited states proceed via $\pi h_{9/2} \rightarrow \nu f_{7/2}, h_{9/2}$ and $\pi f_{7/2} \rightarrow \nu f_{5/2,7/2}, h_{9/2}$, which are impeded by (almost) fully occupied $\nu f_{7/2}, h_{9/2}$ orbitals as well as a small $\pi f_{7/2}$ contribution in the ^{208}At ground state. Allowed β decays populating core-excited states suffer from similar obstructions. In contrast, first-forbidden decays proceeding via $\pi h_{9/2} \rightarrow \nu g_{9/2}, i_{11/2}$ and $\pi s_{1/2}, d_{3/2} \rightarrow \nu p_{1/2}$ are unhindered by the aforementioned factors. These decays populate core-excited negative-parity states with excitation energies of 3–4.5 MeV. These factors contribute to the observed high abundance of first-forbidden decays, particularly at higher energies.

The pandemonium effect [31] refers to the underestimation of β-decay feeding into high-excitation-energy states. It is caused by the low/limited efficiency for the detection of high-energy γ rays. The large crystal size of the HPGe detectors of the IDS allowed for the identification of weak, high-energy transitions, the weakest being at the level of 10^{-4} per β decay. The β-feeding intensity from previous works, compared with the present study, are also shown in Fig. 4. Naturally, experiments in the past were performed with much smaller, less efficient detectors. The largest detector used by Treytl *et al.* [8] in the 1960s was a 32-cm^3 Ge(Li) detector. Consequently no excited states above 2.9 MeV were observed, and the amount of feeding to first-forbidden (negative-parity) states was only $\approx$22% (with $\approx$5% to unknown parity). Experiments in the 1980s were performed with slightly larger Ge(Li) detectors, with volumes of up to 50 cm^3 [5,21] and 13% relative efficiency [7]. Using these detectors more information on high-energy excited states was obtained and thus the fraction of first-forbidden β decays increased to $\approx$37% [14]. In contrast, our clover detectors have crystal sizes of $\approx$250 cm^3 [13]. Using addback their effective size increased significantly. The use of a total absorption spectrometer would clarify the amount of additional pandemonium effect in the results presented here.

By virtue of their structure, many nuclei in the vicinity of ^{208}Po will also exhibit a high proportion of forbidden decays. Allowed transitions are hindered by fully occupied orbitals in the daughter nuclei and an almost empty $\pi f_{7/2}$ in the parent nuclei. First-forbidden decays, however, are not inhibited in this way. Since first-forbidden decays will populate high-energy, excited states, experiments with a high detection efficiency which mitigate the pandemonium effect would show that such decays are more prevalent than previously thought. The number of observed first-forbidden β decays relative to all decays for the region is indicated in Fig. 5. The nuclei ^{207,208}Bi and ^{208,209}Po have low $Q_{\rm EC}$ values such that their daughters have few excited states within the available $Q_{\rm EC}$ window. They therefore decay via the lowest degree(s) of forbiddeness, which is at least first forbidden (as in ^{207}Bi and ^{208}Bi), since allowed β decay cannot take place due to the lack of excited states with the required spin parity in the daughter nuclei. In the decay of ^{208}Po and ^{209}Po not even first-forbidden β decay can take place, for the same reason. The β decay of ^{206}Po is also peculiar. There are no negative-parity states in the daughter nucleus below the $Q_{\rm EC}$ value, consequently all decay proceeds via allowed transitions. For the ^{210}Rn decay, the negative-parity state(s) is(are) just below the $Q_{\rm EC}$ value, making them energetically very unfavorable.

For all other nuclei in the region, first-forbidden decay competes with allowed transitions. In many nuclei the highest-energy observed excited states populated in β decay

are far below the Q_{EC} value, which, in the cases of ^{205}At, ^{206}At, and ^{207}At decay, is a clear indication of the pandemonium effect. The situation is similar in the $^{206-209}$Rn nuclei, for which β-decay data are very scarce.

Understanding competition between allowed and first-forbidden β decay is important for nucleosynthesis [39–41]. Specifically, this is the case for the production of heavy elements in the A $\approx$ 195 r-process abundance peak. For $N = 126$ r-process-path nuclides the first-forbidden decays successfully compete with allowed ones. Since these nuclei are far from stability, there is no experimental information, and the abundance calculations rely on theoretical nuclear properties, However, fundamental properties such as half-lives are difficult to predict, and the predictions that have been made vary significantly [39,40,42–47]. Several global calculations covering the regions of interest for the r-process have been published [39,42,47]. Since shell model calculations are not feasible far from closed shells, all global calculations use mean-field approaches, and all recent studies include first-forbidden decays. Here we suggest that the $N < 126$, $Z > 82$ region provides a good testing ground for such calculations. First-forbidden and allowed transitions compete, and experiments with high yields can be performed in this region, as shown in this example for the β decay of ^{208}At.

VI. CONCLUSIONS

The structure of ^{208}Po was investigated via its population through EC/β^+ decay from the $J^\pi = 6^+$, $Q_{EC} = 5000(9)$ keV [1] ground state of ^{208}At. The ^{208}Po level scheme has been significantly extended. Forty-three previously unreported transitions and 27 new levels have been placed in an expanded level scheme alongside preexisting and (re)assigned transitions and levels. Spin-parity assignments are based on decay patterns, previously measured conversion electron coefficients, and logft values. Comparison with shell model calculations showed a good agreement for non-core-excited states.

First-forbidden decays populate predominantly states at high excitation energies, qualitatively explained by shell model considerations. First-forbidden and allowed β decays have similar yields, which is consistent with other nuclei in the region. The observation of many of the first-forbidden β-decay branches relied on the high detection efficiency for high-energy γ rays. Observations of the β-decay properties of nuclei in the $N < 126$, $Z > 82$ region suggest that ^{208}Po and its neighboring nuclei provide a good testing ground for first-forbidden β-decay calculations, the understanding of which is important for r-process nucleosynthesis.

ACKNOWLEDGMENTS

The authors would like to thank the operators of the ISOLDE facility for providing the beam for this experiment. The research leading to these results received funding from the European Union's Horizon 2020 research and innovation program under Grant Agreement No. 654002. Support from the European Union Seventh Framework through ENSAR Contract No. 262010, as well as the Science and Technology Facilities Council (U.K.) through Grants No. ST/P005314/1, No. ST/L005743/1, No. ST/J000051/1, No. ST/L005670/1, and No. ST/P004598/1, the German BMBF under Contract No. 05P18PKCIA and "Verbundprojekt 05P2018" as well as Spanish MINECO Grants No. FPA2015-65035-P and No. FPA2017-87568-P, FWOVlaanderen (Belgium), GOA/2015/010 (BOF KU Leuven), the Excellence of Science Programme (EOS-FWO), the Interuniversity Attraction Poles Programme initiated by the Belgian Science Policy Office (BriX network P7/12), the Polish National Science Centre under Contracts No. UMO-2015/18/M/ST2/00523 and No. UMO-2019/33/N/ST2/03023, National Science Foundation (U.S.) Grant No. PHY1811855, and the Romanian IFA project CERN-RO/ISOLDE is acknowledged. P.H.R. acknowledges support from the U.K. Department for Business, Energy and Industrial Strategy via the National Measurement Office.

[1] M. Wang *et al.*, Chin. Phys. C **41**, 030003 (2017).
[2] I. Bergstrom *et al.*, Z. Phys. **A287**, 219 (1978).
[3] T. Yamazaki, Phys. Rev. C **1**, 290 (1970).
[4] A. R. Poletti *et al.*, Nucl. Phys. A **615**, 95 (1997).
[5] V. M. Vakhtel *et al.*, Izv. Akad. Nauk SSSR, Ser. Fiz. **45**, 1841 (1981) [Bull. Acad. Sci. USSR, Phys. Ser. **45** (10), 29 (1981)].
[6] B. S. Dzhelepov *et al.*, Izv. Akad. Nauk SSSR, Ser. Fiz. **47**, 2 (1983) [Bull. Acad. Sci. USSR, Phys. Ser. **47**(1), 1 (1983)].
[7] V. Rahkonen and T. Lonnroth, Z. Phys. A. **322**, 333 (1985).
[8] W. J. Treytl, E. K. Hyde, and T. Yamazaki, Nucl. Phys. A **117**, 481 (1968).
[9] E. W. A. Lingeman, Ph.D. thesis, University of Amsterdam, 1975.
[10] R. J. Carroll *et al.*, Phys. Rev. Lett. **125**, 192501 (2020).
[11] T. Stora, Nucl. Instrum. Methods Phys. Res., Sect. B **317**, 402 2013).
[12] M. J. G. Borge and B. Jonson, J. Phys. G: Nucl. Particle Phys. **44**, 044011 (2017).
[13] H. C. Scraggs *et al.*, Nucl. Instrum. Methods Phys. Res. Sec. A **543**, 431 (2005).
[14] M. J. Martin, Nucl. Data Sheets **108**, 1583 (2007).
[15] I. Lazarus *et al.*, IEEE Trans. Nucl. Sci. **48**, 567 (2001).
[16] T. A. Berry, Ph.D. thesis, University of Surrey, 2019.
[17] M. Brunet, Ph.D. thesis, University of Surrey, 2021.
[18] M. Brunet *et al.*, J. Phys. Conf. Ser. **1643**, 012116 (2020).
[19] G. R. Gilmore, *Practical γ-Ray Spectrometry* (John Wiley & Sons, Chichester, UK, 2008), p. 361.
[20] F. G. Kondev and S. Lalkovski, Nucl. Data Sheets **112**, 707 (2011).
[21] B. S. Dzhelepov *et al.*, Program and Thesis in *33rd Annual Conf. Nucl. Spectrosc. Struct. At. Nuclei* (Moscow, 1983), p. 152.
[22] B. Singh *et al.*, Nucl. Data Sheets **84**, 487 (1998).
[23] T. Kibédi, T. Burrows *et al.*, Nucl. Instrum. Methods Phys. Res. Sec. A **589**, 202 (2008).
[24] B. A. Brown and W. D. M. Rae, Nucl. Data Sheets **120**, 115 (2014).

[25] E. K. Warburton and B. A. Brown, Phys. Rev. C **43**, 602 (1991).
[26] W. G. Love, *The (p, n) Reaction and the Nucleon-Nucleon Force* (Plenum, New York, 1980), p. 23.
[27] G. Bertsch *et al.*, Nucl. Phys. A **284**, 399 (1977).
[28] B. A. Brown, Phys. Rev. C **58**, 220 (1998).
[29] G. Astner *et al.*, Nucl. Phys. A **182**, 219 (1972).
[30] M. Brunet *et al.* (Unpublished) (2021).
[31] J. C. Hardy *et al.*, Phys. Lett. B **71**, 307 (1977).
[32] F. G. Kondev, Nucl. Data Sheets **105**, 1 (2005).
[33] C. J. Chiara and F. G. Kondev, Nucl. Data Sheets **111**, 141 (2010).
[34] F. G. Kondev, Nucl. Data Sheets **166**, 1 (2020).
[35] F. G. Kondev, Nucl. Data Sheets **109**, 1527 (2008).
[36] J. Chen and F. G. Kondev, Nucl. Data Sheets **126**, 373 (2015).
[37] M. Shamsuzzoha Basunia, Nucl. Data Sheets **121**, 561 (2014).
[38] B. Singh *et al.*, Nucl. Data Sheets **114**, 661 (2013).
[39] P. Möller, B. Pfeiffer, and K. L. Kratz, Phys. Rev. C **67**, 055802 (2003).
[40] D. L. Fang, B. A. Brown, and T. Suzuki, Phys. Rev. C **88**, 034304 (2013).
[41] N. Nishimura *et al.*, Phys. Lett. B **756**, 273 (2016).
[42] E. M. Ney, J. Engel, T. Li, and N. Schunck, Phys. Rev. C **102**, 034326 (2020).
[43] H. Koura *et al.*, Prog. Theor. Phys. **113**, 305 (2005).
[44] I. N. Borzov, Nucl. Phys. A **777**, 645 (2006).
[45] T. Suzuki, T. Yoshida, T. Kajino, and T. Otsuka, Phys. Rev. C **85**, 015802 (2012).
[46] Q. Zhi, E. Caurier, J. J. Cuenca-Garcia, K. Langanke, G. Martinez-Pinedo, and K. Sieja, Phys. Rev. C **87**, 025803 (2013).
[47] T. Marketin, L. Huther, and G. Martinez-Pinedo, Phys. Rev. C **93**, 025805 (2016).
[48] O. Dragoun *et al.*, Czech. J. Phys. **B32**, 711 (1982).
[49] O. Dragoun *et al.*, Nucl. Phys. A **391**, 29 (1982).